ISSN 1674-1056
http://cpb.iphy.ac.cn
http://iopscience.iop.org/cpb
中国物理 B
Chinese Physics
中国物理
Chinese Physics B

High-pressure synchrotron x-ray diffraction and Raman spectroscopic study of plumbogummite

Duan Kang(康端), Xiang Wu(巫翔), Guan Yuan(袁冠), Sheng-Xuan Huang(黄圣轩), Jing-Jing Niu(牛菁菁), Jing Gao(高静), Shan Qin(秦善)
Citation: Chin. Phys. B . 2018, 27(1): 017402. **doi:** 10.1088/1674-1056/27/1/017402

Journal homepage: http://cpb.iphy.ac.cn; http://iopscience.iop.org/cpb

What follows is a list of articles you may be interested in

Structural, elastic, and vibrational properties of phase H: A first-principles simulation

Chao-Jia Lv(吕超甲), Lei Liu(刘雷), Yang Gao(高阳), Hong Liu(刘红), Li Yi(易丽), Chun-Qiang Zhuang(庄春强), Ying Li(李营), Jian-Guo Du(杜建国)
Chin. Phys. B . 2017, 26(6): 067401. **doi:** 10.1088/1674-1056/26/6/067401

Quantitative analysis of ammonium salts in coking industrial liquid waste treatment process based on Raman spectroscopy

Ya-Nan Cao(曹亚南), Gui-Shi Wang(王贵师), Tu Tan(谈图), Ting-Dong Cai(蔡廷栋), Kun Liu(刘锟), Lei Wang(汪磊), Gong-Dong Zhu(朱公栋), Jiao-Xu Mei(梅教旭)
Chin. Phys. B . 2016, 25(10): 107403. **doi:** 10.1088/1674-1056/25/10/107403

High-pressure Raman study of solid hydrogen up to 300 GPa

Xiaoli Huang(黄晓丽), Fangfei Li(李芳菲), Yanping Huang(黄艳萍), Gang Wu(吴刚), Xin Li(李鑫), Qiang Zhou(周强), Bingbing Liu(刘冰冰), Tian Cui(崔田)
Chin. Phys. B . 2016, 25(3): 037401. **doi:** 10.1088/1674-1056/25/3/037401

First-principles simulation of Raman spectra and structural properties of quartz up to 5 GPa

Liu Lei, Lv Chao-Jia, Zhuang Chun-Qiang, Yi Li, Liu Hong, Du Jian-Guo
Chin. Phys. B . 2015, 24(12): 127401. **doi:** 10.1088/1674-1056/24/12/127401

High-sensitive automatic transient laser-induced breakdown spectroscopy system with high temporal and spatial resolution

Liu Qiao-Jun, S. K. Fong, Andrew Y. S. Cheng, Luo Shi-Rong, K. S. Tam, Zhu Jian-Hua, A. Viseu
Chin. Phys. B . 2012, 21(8): 087402. **doi:** 10.1088/1674-1056/21/8/087402

High-pressure synchrotron x-ray diffraction and Raman spectroscopic study of plumbogummite*

Duan Kang(康端)[1], Xiang Wu(巫翔)[2,†], Guan Yuan(袁冠)[1], Sheng-Xuan Huang(黄圣轩)[1], Jing-Jing Niu(牛菁菁)[1], Jing Gao(高静)[1], and Shan Qin(秦善)[1]

[1] *Key Laboratory of Orogenic Belts and Crustal Evolution, Ministry of Education, School of Earth and Space Sciences, Peking University, Beijing* 100871, *China*

[2] *State Key Laboratory of Geological Processes and Mineral Resources, China University of Geosciences, Wuhan* 430074, *China*

(Received 18 April 2017; revised manuscript received 18 October 2017; published online 10 December 2017)

$PbAl_3(PO_4)_2(OH,H_2O)_6$, an important environmental mineral, is in-situ studied by synchrotron x-ray diffraction (XRD) and Raman scattering combined with diamond anvil cells (DACs) at pressures up to ~11.0 GPa and room temperature. The XRD results indicate that plumbogummite does not undergo a phase transition between 0 GPa and 10.9 GPa. Moreover, the *c* axis is more compressible than the *a* axis, revealing its anisotropic behavior. The pressure-volume data are fitted to the third-order Birch-Murnaghan equation of state to yield the plumbogummite bulk modulus K_0 of 68(1) GPa and K_0' of 6.1. The $[PO_4]^{3-}$ and $[HPO_4]^{2-}$ Raman vibrational modes exhibit scale nearly linearly as a function of pressure. The $[PO_4]^{3-}$ stretching modes are generally more sensitive to pressure than the bending modes. The Grüneisen parameters range from −0.07 to 1.19, with an arithmetic mean of approximately 0.39.

Keywords: plumbogummite, equation of state, Grüneisen parameter, diamond anvil cell

PACS: 74.25.nd, 74.25.Ld **DOI:** 10.1088/1674-1056/27/1/017402

1. Introduction

Plumbogummite group is an important phosphorus source and can be found in sedimentary, igneous, and metamorphic rocks and in soils.[1–3] Its chemical formula is $XAl_3(PO_4)_2(OH, H_2O)_6$, where *X* can be Ca, Sr, Ba, Pb, or a rare earth element.[4] Plumbogummite is the prototype mineral with the chemical formula $PbAl_3(PO_4)_2(OH, H_2O)_6$. It is thermodynamically stable on the Earth's surface[5,6] and is the predominant Pb mineral in soils, accounting for 43–51% of their total Pb content.[3] The plumbogummite crystal phase is trigonal with a space group of $R\bar{3}m$, $Z = 3$.[7] The Pb atoms in plumbogummite are disordered and distributed among six sites, each with a 1/6 occupancy. The six sites are confined to the (0001) plane and centered around the position (0.0409, 0.0409, 0) (Fig. 1(a)).[8] In this mineral, corner-sharing AlO_6 octahedra form layers that are linked by distorted PbO_{12} polyhedra. The Pb-O and Pb-Al distances in these polyhedra vary, resulting in asymmetric Pb polyhedra in which the Pb atoms are off-center. This structure is also observed in other Pb crandallites such as hinsdalite.[8] In addition, PO_4 tetrahedra are distributed between the AlO_6 octahedra layers, and each PO_4 tetrahedron is connected to three AlO_6 octahedra that are in the same layer via corner linkages (Fig. 1(b)).

XRD and Raman spectroscopy are powerful techniques for exploring structural and vibrational properties.[9–13] Several XRD and/or Raman investigations of $[PO_4]^{3-}$-containing minerals have appeared in the literature.[14,15] For example, high-pressure Raman scattering was employed to determine the changes in the structure and pressure coefficients of the phosphate modes in $Ba_3(PO_4)_2$, $Sr_3(PO_4)_2$, and $K_2MgWO_2(PO_4)_2$.[16,17] Moreover, the axial compressibilities and bulk moduli of $Sr_3(PO_4)_2$ and $Pb_3(PO_4)_2$ were obtained from high-pressure XRD experiments.[18,19]

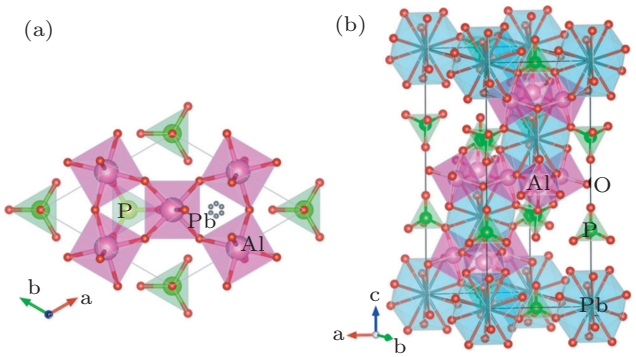


Fig. 1. (color online) Plumbogummite Crystal structures (Al: magenta; P: green; O: red). Representations of (a) the six Pb sites (gray spheres), each with a 1/6 occupancy, and (b) one of the six Pb sites showing the PbO_{12} polyhedron.

Frost *et al.* first analyzed plumbogummite by Raman scattering at ambient temperature and pressure.[20] Minerals containing Al^{3+} cations and $[OH]^-$ and $[PO_4]^{3-}$ groups, such as taranakite $((K,NH_4)Al_3(PO_4)_3(OH)\cdot 9(H_2O))$,[21] florencite-La $(LaAl_3(PO_4)_2(OH,H_2O)_6)$,[22] and wardite $(NaAl_3(PO_4)_2(OH)_2\cdot 2(H_2O))$,[23] have also been extensively studied by Raman scattering under am-

*Project supported by the National Natural Science Foundation of China (Grant Nos. 41473056 and 41472037).

†Corresponding author. E-mail: wuxiang@cug.edu.cn

© 2018 Chinese Physical Society and IOP Publishing Ltd

bient conditions. Similarly, many minerals containing Fe^{3+} cations and $[OH]^{-}$ and $[PO_4]^{3-}$ groups, such as delvauxite ($CaFe_4^{3+}(PO_4,SO_4)_2(OH)_8\cdot$ 4-6(H_2O)),[24] frondelite ($(Mn^{2+})(Fe^{3+})_4(PO_4)_3(OH)_5$),[25] and leucophosphite ($K(Fe^{3+})_2(PO_4)_2(OH)\cdot$ 2(H_2O)),[26] have also been investigated by Raman spectroscopy. These minerals have similar Raman spectra, and their Raman modes have been assigned, providing reliable references for this high-pressure Raman study of plumbogummite.

XRD studies of plumbogummite were conducted under ambient conditions to determine its structure.[4,27–29] However, unlike minerals containing only $[PO_4]^{3-}$ groups, which have been extensively studied under high-pressure conditions, only a few high-pressure XRD and Raman investigations of plumbogummite-type minerals, even those containing $[OH]^{-}$ and $[PO_4]^{3-}$ groups, have been performed. To study the high-pressure behavior of plumbogummite, high-pressure synchrotron XRD and Raman scattering studies were performed *in situ* in a DAC at pressures ranging from 0 GPa to approximately 11.0 GPa to simulate hydrostatic pressure. The axial compressibilities, bulk moduli and changes in the Raman vibrational modes of plumbogummite at room temperature and high pressures were determined from the experimental results.

2. Experiments

A natural plumbogummite sample was purchased from a trustworthy market; however, the place of origin was unknown. The plumbogummite structure under ambient conditions was characterized by XRD, and all the peaks were indexed to a trigonal phase with lattice constants of $a = 7.015(1)$ Å, $c = 16.668(2)$ Å, and $V = 710.3(1)$ Å^3, which are in good agreement with previously reported values.[4,8,27] Furthermore, the Raman spectrum obtained under ambient conditions is in good agreement with the spectrum in the RRUFF database (ID: R050458), confirming the purity of the single-phase sample.

Symmetrical DACs with 300 μm-diameter culets were employed to create high pressures. The sample chambers consisted of ∼150 μm-diameter holes drilled into Re gasket, which were preindented to a depth of of ∼ 40 μm. A thin sample was loaded into the sample chamber with a 4:1 methanol:ethanol mixture as the pressure medium. Au foil and a tiny ruby sphere[30] were employed to calibrate the pressure in the XRD and Raman scattering experiments, respectively.

Zero- and high-pressure XRD experiments were performed at beamline 15U at Shanghai Synchrotron Radiation Facility (SSRF). A monochromatic x-ray beam with a wavelength of 0.6199 Å was focused on a 3×4 μm^2 spot. The XRD patterns were recorded with a Mar charge-coupled device (CCD) detector using an exposure time of 200 s. All the collected images were integrated using the Fit2D program to obtain conventional one-dimensional diffraction patterns.[31] The lattice parameters were refined by the LeBail method implemented in the GSAS+EXPGUI software.[32] High-pressure Raman spectroscopy experiments were performed *in situ* using a Renishaw Invia Reflex Raman spectrometer at Peking University. A 785 nm diode-pumped solid-state laser with a ∼ 2.5 μm focused beam was employed as the excitation light source. The spectra were calibrated by using silicon wafer, and the backscattered light was collected by a CCD detector with a resolution of 1 cm^{-1}. Two 200 s scans were performed to obtain each spectrum. The Raman spectra were fitted by the Gauss-Lorentzian method using the Peakfit software (Jandel Scientific).

3. Results and discussion

3.1. High-pressure XRD experiments

Plumbogummite XRD patterns are collected at room temperature at pressures up to 10.9 GPa. Figure 2 shows several representative XRD patterns. All the peaks can be indexed to the $R\bar{3}m$ space group. Compression of the sample results in a shift in all the diffraction peaks to higher angles (Fig. 2), indicating a decrease in the plumbogummite volume. At the same time, the diffraction peak intensities decrease, and their full widths at half maximum increase slightly with increasing pressure. In a pressure range of 0–10.9 GPa, no new diffraction peaks appear, and none of original peaks disappear, indicating that plumbogummite is stable at pressures up to 10.9 GPa at room temperature.

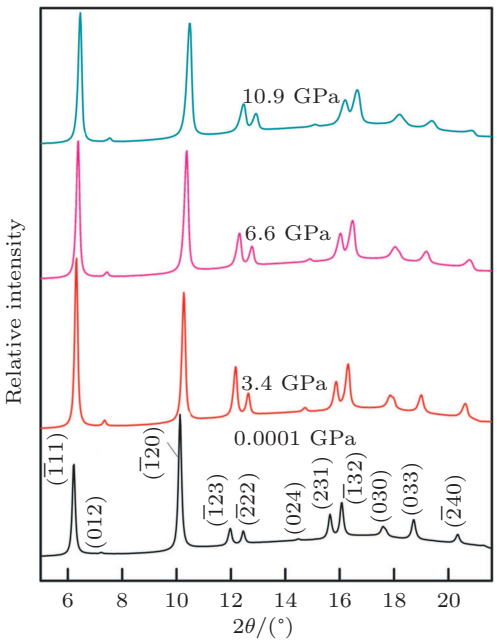


Fig. 2. (color online) Selected plumbogummite XRD patterns obtained at room temperature and various pressures (background subtracted). The peaks in the XRD pattern obtained at ambient pressure are marked with the corresponding *hkl* values.

The plumbogummite lattice parameters measured at different pressures are listed in Table 1, and the normalized lattice parameters are shown as a function of pressure in Fig. 3. Linear regression of the data in Fig. 3 gives the following correlations between the normalized lattice parameters and pressure (P): $a/a_0 = 0.9982(6) - 2.8 \times 10^{-3}$ (GPa^{-1}) $\times P$ (GPa) and $c/c_0 = 0.9965(9) - 4.5 \times 10^{-3}$ (GPa^{-1}) $\times P$ (GPa). The compressibility of plumbogummite is slightly anisotropic in the pressure range of 0–10.9 GPa; the compressibility along the c axis is greater than that along the a axis (Fig. 3) because the atoms are more closely packed along the a axis than along the c axis. As the pressure increases from 0 GPa to 10.9 GPa, the a and c axes decrease in length by 3.12% and 5.02%, respectively.

Table 1. Plumbogummite lattice parameters at different pressures.

Pressure/GPa	a/Å	c/Å	V/Å^3
0.0001	7.015(1)	16.668(2)	710.3(1)
1.8	6.970(1)	16.482(2)	693.4(1)
2.4	6.953(1)	16.424(2)	687.6(1)
3.4	6.932(1)	16.326(2)	679.3(1)
4.3	6.913(1)	16.258(2)	672.9(1)
5.1	6.896(1)	16.210(2)	667.5(1)
5.8	6.881(1)	16.166(2)	662.9(1)
6.6	6.868(1)	16.087(2)	657.1(1)
8.2	6.842(1)	15.994(2)	648.4(1)
9.5	6.825(1)	15.921(2)	642.2(1)
10.9	6.796(1)	15.831(2)	633.3(1)

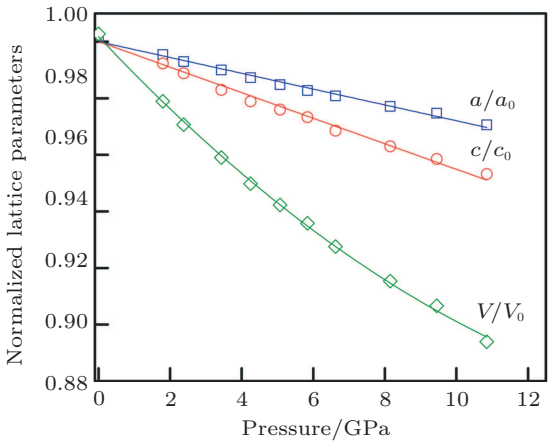


Fig. 3. (color online) Normalized plumbogummite lattice parameters a/a_0 and c/c_0 as a function of pressure. The blue and red lines are fitted by the least-squares method, and the green line represents the fitted second-order Birch-Murnaghan equation with $K_0 = 77$ GPa.

The correlation between the plumbogummite unit cell volume and the pressure is obtained by fitting the third-order Birch-Murnaghan equation of state to the data:[33]

$$P(V) = 1.5K_0\left[\left(\frac{V_0}{V}\right)^{7/3} - \left(\frac{V_0}{V}\right)^{5/3}\right] \times \left\{1 + 0.75(K_0' - 4)\left[\left(\frac{V_0}{V}\right)^{2/3} - 1\right]\right\}, \quad (1)$$

where V_0 is the unit cell volume at ambient pressure, K_0 is the zero-pressure bulk modulus, and K_0' is the pressure derivative of K_0. The fitted equation gives $V_0 = 710.2(1)$ Å^3 and $K_0 = 68(1)$ GPa ($K_0' = 6.1$) for plumbogummite. When K_0' is set to be 4, equation (1) becomes the second-order Birch-Murnaghan equation, and V_0 and K_0 are determined to be 708.4(1) Å^3 and 77(1) GPa, respectively. To the best of our knowledge, the zero-pressure bulk moduli of minerals containing $[PO_4]^{3-}$ and $[OH]^-$ groups have not been previously measured, except in the case of orthorhombic $Cu_2PO_4(OH)$, which was reported to have a K_0 value of 60 GPa ($K_0' = 4.8$).[34] Based on the small K_0 values determined for $Cu_2PO_4(OH)$ and $PbAl_3(PO_4)_2(OH,H_2O)_6$, it is assumed that minerals containing $[PO_4]^{3-}$ and $[OH]^-$ groups are easily compressed.

3.2. High-pressure Raman spectroscopy

Raman spectra of plumbogummite were collected in a range of 150–1250 cm^{-1} at various pressures (Fig. 4). Sixteen peaks can be identified in the spectrum obtained at ambient pressure, which is consistent with the Raman spectra reported in the RRUFF database and previous studies.[20] Due to the overlap of some Raman bands, the fitted plumbogummite Raman profiles obtained at pressures of 0 GPa and 2.6 GPa are shown in Fig. 5 to demonstrate the band positions more clearly. A new peak is observed at 393 cm^{-1} when the pressure is 2.6 GPa or higher. This peak might also exist at 0 GPa; however, it is too weak or too close to the peak at 369 cm^{-1} to be observed. As the pressure increases, the bands at 369 and 393 cm^{-1} shift at different rates, which makes the 393 cm^{-1} peak easy to observe at 2.6 GPa. In a previous study, a band was observed at 388 cm^{-1} for a plumbogummite sample from China but not for a sample from Czech Republic.[20] Furthermore, the 388 cm^{-1} band observed in the Raman spectrum of the Chinese sample was weak and very close to the 368 cm^{-1} band, indicating that the band at 388 cm^{-1} is difficult to detect under ambient conditions. Moreover, the band at 712 cm^{-1} is observed only at pressures of 0.0001, 4.7, 5.4, 6.5, and 11.0 GPa.

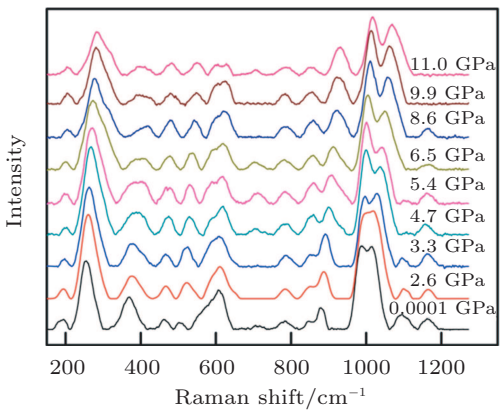


Fig. 4. (color online) Raman spectra of plumbogummite obtained at room temperature and different pressures (baselines substracted).

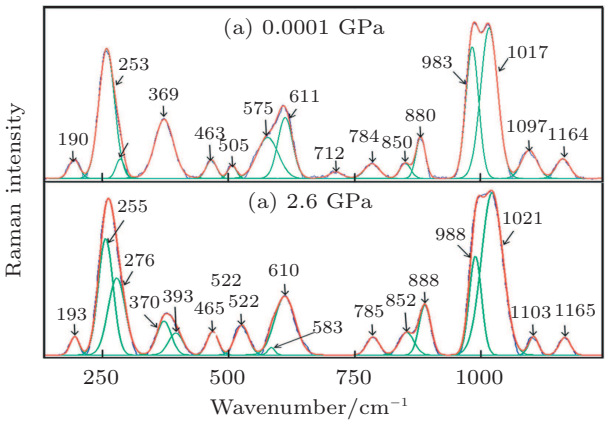


Fig. 5. (color online) Fitted plumbogummite Raman profiles obtained at pressures of (a) 0 GPa and (b) 2.6 GPa (thin blue lines: experimental Raman spectra; green lines: fitted peaks; red lines: entire fitted Raman profiles obtained by the superposition of the fitted peaks).

A regular PO_4 tetrahedron exhibits Raman vibrational modes at 938 cm^{-1} (ν_1), 420 cm^{-1} (ν_2), 1017 cm^{-1} (ν_3) and 515 cm^{-1} (ν_4).[35] When the hydroxyl hydrogens in plumbogummite are mobile, they can interact with the phosphate $[PO_4]^{3-}$ groups to generate hydrogen phosphate $[HPO_4]^{2-}$.[36] However, the $[PO_4]^{3-}$ and $[HPO_4]^{2-}$ Raman peaks should have the same frequencies, giving rise to wide bands.[20] Therefore, the plumbogummite Raman peak assignment suffers uncertainties in the $[PO_4]^{3-}$ and $[HPO_4]^{2-}$ vibrational modes. Fortunately, Breitinger *et al.*[37] definitively separated the $[PO_4]^{3-}$ and $[HPO_4]^{2-}$ vibrations of crandallite ($CaAl_3(OH)_6(HPO_4)(PO_4)$) and goyazite ($SrAl_3(OH)_6(HPO_4)(PO_4)$) by combining infrared, Raman and inelastic neutron scattering results. In this study, the Raman modes are assigned mainly based on the normal modes of a regular PO_4 tetrahedron reported in previous Raman studies of plumbogummite,[20] crandallite, and goyazite.[38] The positions and vibrational mode assignments of the plumbogummite Raman peaks observed at room temperature and different pressures are listed in Table 2.

Table 2. Peak positions, values of pressure derivative ($d\nu_i/dP$) and Grüneisen parameter (γ_i) of the plumbogummite Raman modes observed at different pressures.

Mode Assignment	Pressure/GPa									$d\nu_i/dP$ (cm^{-1}/GPa)	γ_i
	0	2.6	3.3	4.7	5.4	6.5	8.6	9.9	11.0		
Lattice mode	190	193	196	199	200	199	204	205	204	1.39	0.56
Lattice mode/$[OH]^-$	253	255	259	266	268	269	278	279	285	3.05	0.93
Lattice mode/$[OH]^-$	279	276	285	299	299	307	317	311	321	4.30	1.19
ν(Pb-O)/ν(Al-O)	369	370	376	377	377	385	406	396	397	3.30	0.69
ν(Pb-O)/ν(Al-O)		393	406	406	410	411	421	424	421	3.14	0.62
$\delta_s[PO_4]^{3-}$	463	465	467	473	474	475	479	481	480	1.80	0.30
$\delta_s[HPO_4]^{2-}$	505	522	523	531	531	535	544	547	549	3.85	0.59
$\delta_{as}[PO_4]^{3--}$	575	583	583	587	586	588	595	603	602	2.51	0.34
$\delta_{as}[PO_4]^{3-}$	611	610	612	617	617	620	624	629	628	1.92	0.24
OH deformation mode	712			706	711	705			705	−0.65	−0.07
	784	785	788	784	785	783	784	783	786	−0.08	−0.01
Water vibrational mode	850	852	853	854	857	856	855	852	854	0.26	0.02
Water vibrational mode	880	888	891	902	909	914	923	926	930	4.93	0.43
$\nu_s[HPO_4]^{2-}$	983	988	991	997	999	1003	1010	1012	1016	3.15	0.25
$\nu_s[PO_4]^{3-}$	1017	1021	1028	1038	1041	1050	1060	1064	1072	5.36	0.41
$\nu_{as}[HPO_4]^{2-}$	1097	1103	1100	1113	1108					2.52	0.18
$\nu_{as}[PO_4]^{3-}$	1164	1165	1167	1161	1164	1165	1164			−0.09	−0.01

Note: ν_s and ν_{as} represent symmetric and asymmetric stretching modes, respectively; δ_s and δ_{as} represent symmetric and asymmetric bending vibrational modes, respectively.

The predominant bands in the plumbogummite Raman spectrum are due to the $[PO_4]^{3-}$ and $[HPO_4]^{2-}$ vibrational modes. The Raman bands at 190, 253, and 279 cm^{-1} are due to lattice vibrations, and the peaks at 253 and 279 cm^{-1} might be associated with the $[OH]^-$ group. The Pb-O and Al-O stretching modes are observed at 369 and 393 cm^{-1}, respectively. The symmetric bending modes of $[PO_4]^{3-}$($\nu_2(\delta_s)[PO_4]^{3-}$) and $[HPO_4]^{2-}$ ($\nu_2(\delta_s)[HPO_4]^{2-}$) are observed at 463 and 505 cm^{-1}, respectively. The $[PO_4]^{3-}$ asymmetric bending modes ($\nu_4(\delta_{as})[PO_4]^{3-}$) appear at 575 and 611 cm^{-1}, and the band at 712 cm^{-1} corresponds to the $[OH]^-$ deformation mode. However, the band at 784 cm^{-1} is not assigned to a specific mode. The bands at 852 and 880 cm^{-1} are attributed to the vibrational modes of water, which is consistent with the assignments of the bands at 816 and 877 cm^{-1} for (Mn, Fe)$Al(PO_4)(OH)_2\cdot(H_2O)$.[38]

Although Frost *et al.*[20] assigned the plumbogummite bands at 980 and 1023 cm^{-1} to $\nu_1(\nu_s)[PO_4]^{3-}$ and $\nu_1(\nu_s)[HPO_4]^{2-}$, respectively, the bands observed at 981 and 1012 cm^{-1} for montgomeryite mineral ($Ca_4MgAl_4(PO_4)_6\cdot(OH)_4\cdot 12H_2O$) were assigned to $\nu_1[HPO_4]^{2-}$ and $\nu_1[PO_4]^{3-}$, respectively.[39] Moreover, Breitinger *et al.*[37] reported that the crandallite ($CaAl_3(OH)_6(HPO_4)(PO_4)$) bands at 982 and 1035 cm^{-1} are due to the $\nu_1[HPO_4]^{2-}$ and $\nu_1[PO_4]^{3-}$ symmetric stretching vibrations, respectively. Consequently, the intense sharp bands at 983 and 1017 cm^{-1} in the plumbogummite Raman spectrum are attributed to $\nu_1[HPO_4]^{2-}$ and $\nu_1[PO_4]^{3-}$, respectively. Two weaker bands corresponding to the $[HPO_4]^{2-}$ ($\nu_3(\nu_{as})[HPO_4]^{2-}$) and $[PO_4]^{3-}$ ($\nu_3(\nu_{as})[PO_4]^{3-}$) asymmetric stretching modes are observed

to the right of these bands at 1097 and 1164 cm^{-1}, respectively.

Frost *et al.*[20] observed a series of Raman peaks due to the $[OH]^-$ stretching vibrations in a range of 2800–3800 cm^{-1}. In this study, Raman data are not collected in this range.

Figure 4 shows the Raman spectra of plumbogummite obtained at different pressures. Most of the Raman peaks widen and undergo a blueshift with increasing pressure, indicating that the atom distances in the lattice change during pressurization.[40] The Raman band intensities gradually decrease to varying degrees due to the restricted lattice vibrations and a decrease in the Raman activity during compression. Figure 6 shows the Raman peak positions as a function of pressure. Most of the Raman peak positions exhibit good linear correlations with the pressure. Therefore, the data are fitted by linear equations, and the slopes of the fitted lines are listed in Table 2.

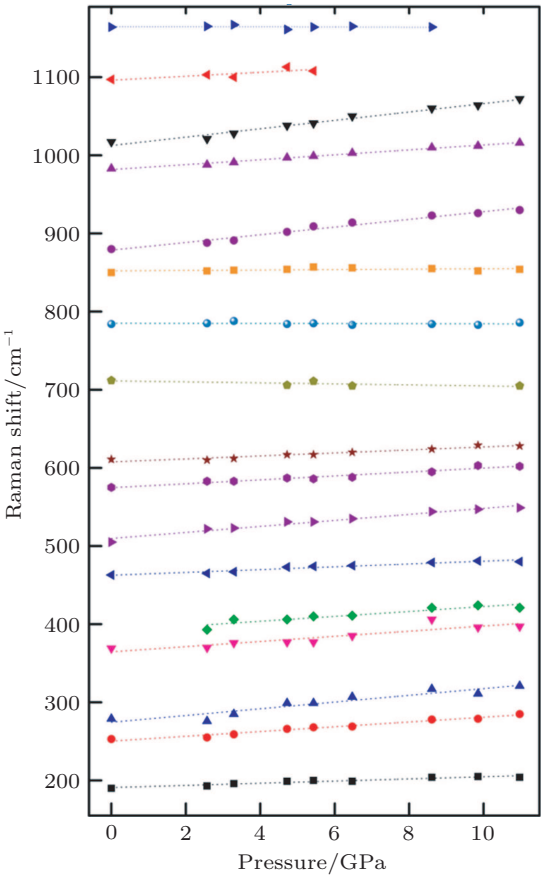


Fig. 6. (color online) Plumbogummite Raman peak positions as a function of pressure. The slopes of the dotted lines, which are the linear least-squares fitting of the data, are the dv_i/dP values.

The Raman band at 712 cm^{-1} undergoes a small shift to lower wavenumbers, implying that the O-H bond in $[OH]^-$ group becomes slightly longer as pressure increases. Most of the vibrational modes of $[PO_4]^{3-}$ group are blue-shifted with pressurization, indicating that the bond lengths in $[PO_4]^{3-}$ group become shorter. However, the Raman band at 1164 cm^{-1} ($\nu_{as}[PO_4]^{3-}$) has a very slight redshift. This may be due to the distortion of $[PO_4]^{3-}$group, resulting in some bonds in $[PO_4]^{3-}$ group shortening to some extent. The Raman peak at 852 cm^{-1} shifts to a higher wavenumber as the applied pressure increases (Fig. 6). Meanwhile, the other Raman peaks are blue-shifted at different rates during pressurization due to the decrease of bond length and the increase of the bond energy. The bands at 1092 and 1164 cm^{-1} are observed only at pressures below 6.5 and 9.9 GPa, respectively. As indicated by the XRD results, plumbogummite does not undergo a phase transition during pressurization up to 10.9 GPa, and all the Raman bands shift constantly without any discontinuities (Fig. 6). The disappearances of the bands at 1092 and 1164 cm^{-1} are likely to be due to structural deformations rather than phase transitions and indicate the destabilization of plumbogummite. Additionally, except for the band at 1164 cm^{-1}, the shifts in the $[PO_4]^{3-}$ bending modes are generally smaller than those in the stretching modes during pressurization. These results suggest that the $[PO_4]^{3-}$ stretching modes are more sensitive to the pressure than the bending modes and that the pressure has a slightly larger effect on the bond lengths than on the bond angle of the PO_4 tetrahedron. Zhai *et al.*[16,41] also reported that the PO_4 stretching modes in $Ba_3(PO_4)_2$, $Sr_3(PO_4)_2$ and γ-$Ca_3(PO_4)_2$ are more sensitive to the pressure than the bending modes.

The Grüneisen parameter (γ_i), which characterizes the anharmonicity of the lattice vibrations, is an important geophysical parameter.[42] It can be expressed as a function of the bulk modulus, Raman frequency and pressure dependence of the frequency as follows:

$$\gamma_i = -\frac{\partial \ln \nu_i}{\partial \ln V} = \frac{K_0}{\nu_{0i}} \left(\frac{\partial \nu_i}{\partial P} \right)_T . \quad (2)$$

In this equation, K_0 is the isothermal bulk modulus of plumbogummite at ambient pressure, ν_{0i} is the Raman frequency of mode i at ambient pressure, and $(\nu_i/P)_T$ is the change in the Raman frequency with respect to pressure under isothermal conditions. The Grüneisen parameters (Table 2) for all the Raman vibrational modes are calculated from the pressure shift coefficients $(\nu_i/P)_T$ in Table 2 and the K_0 value (77(1) GPa) obtained from the XRD results. The Grüneisen parameter for the 393 cm^{-1} mode, which appears when the pressure increases to 2.6 GPa, is calculated using 393 cm^{-1} as ν_{0i}. The Grüneisen parameters for the 712, 784, and 1164 cm^{-1} bands are negative, whereas those for all the other modes are in a range of 0.02–1.19. The average of all the Grüneisen parameters is 0.39. Except for the Grüneisen parameter for the 1164 cm^{-1} mode (−0.01), the Grüneisen parameters associated with the phosphate vibrational modes range from 0.24 to 0.41, with an average of approximately 0.32. Similarly, the Grüneisen parameters associated with the

phosphate vibrational modes in fluorapatite ($Ca_5(PO_4)_3F_2$) were reported to range from 0.09 to 0.55, with an average of 0.36.[43]

4. Conclusions

The high-pressure behavior of plumbogummite is investigated by synchrotron radiation XRD and Raman spectroscopy experiments at room temperature using DACs. The results show that plumbogummite does not undergo a phase transition in the pressure range of 0–10.9 GPa. Moreover, the compressibility of the c axis is higher than that of the a axis in this pressure range. The data are fitted with the third-order Birch-Murnaghan equation of state to give the following results: $V_0 = 710.2(1)$ Å^3, $K_0 = 68(1)$ GPa, and $K_0' = 6.1$.

In the plumbogummite Raman spectrum, the $[PO_4]^{3-}$ symmetric (ν_1) and asymmetric (ν_3) stretching modes are observed at 1017 and 1164 cm^{-1}, respectively. Moreover, the $[PO_4]^{3-}$ symmetric bending mode (ν_2) is observed at 463 cm^{-1}, and the asymmetric bending modes (ν_4) are observed at 575 and 611 cm^{-1}. The bands at 983, 505 and 1097 cm^{-1} correspond to $\nu_1[HPO_4]^{2-}$, $\nu_2[HPO_4]^{2-}$ and $\nu_3[HPO_4]^{2-}$, respectively. Linear functions are fitted to the high-pressure Raman data to determine the dependence of the Raman peak positions on the pressure. Most of the linear functions have positive slopes. A comparison among the changes in the Raman modes as a function of pressure shows that the PO_4 stretching modes are generally more pressure-sensitive than the bending modes. In addition, the arithmetic mean of all the mode Grüneisen parameters for the Raman vibrational modes is 0.39.

Acknowledgment

We thank Ying Wang for her help with the high-pressure XRD experiments.

References

[1] Rattray K J, Taylor M R, Bevan D J M and Pring A 1996 *Mineral. Mag.* **60** 779
[2] Dill H G 2001 *Earth-Sci. Rev.* **53** 35
[3] Morin G 2001 *Am. Mineral.* **86** 92
[4] Grey I E, Shanks F L, Wilson N C, Mumme W G and Birch W D 2011 *Mineral. Mag.* **75** 145
[5] Schwab R G, Götz C, Herold H and Pinto de Oliveira N 1991 *Neues Jahrbuch für Mineralogie Monatshefte* 97
[6] Eighmy T T, Crannell B S, Butler L G, Cartledge F K, Emery E F, Oblas D, Krzanowski J E, Eusden J D, Shaw E L and Francis C A 1997 *Environ. Sci. Technol.* **31** 3330
[7] Kolitsch U and Pring A 2001 *J. Miner. Petrol. Sci.* **96** 67
[8] Kolitsch U, Tiekink E R T, Slade P G, Taylor M R and Pring A 1999 *Eur. J. Mineral.* **11** 513
[9] Jiang J L, Wang Y B, Wang Q, Huang H, Wei Z Q and Hao J Y 2016 *Chin. Phys. B* **25** 048101
[10] Liang H, Peng F, Fan C, Zhang Q, Liu J and Guan S X 2017 *Chin. Phys. B* **26** 053101
[11] Geng A H, Cao L H, Ma Y M, Cui Q L and Wan C M 2016 *Chin. Phys. Lett.* **33** 097401
[12] Cheng H, Li Y C, Li G and Li X D 2016 *Chin. Phys. Lett.* **33** 096104
[13] Yang S W, Peng F, Li W T, Hu Q W, Yan X Z, Lei L, Li X D and He D W 2016 *Chin. Phys. B* **25** 076101
[14] Zhang J, Wang D, Zhang D M, Zhang Q L, Wan S M, Sun D L, Yin S T 2013 *Acta Phys. Sin.* **62** 097802 (in Chinese)
[15] Zhou H L, Gu Q T, Zhang Q H, Liu B A, Zhu L L, Zhang L S, Zhang F, Xu X G, Wang Z P, Sun X and Zhao X 2015 *Acta Phys. Sin.* **64** 197801 (in Chinese)
[16] Zhai S, Liu A, Xue W and Song Y 2011 *Solid State Commun.* **151** 276
[17] Maczka M, Paraguassu W, Filho A G S, Freire P T C, Majchrowski A, Filho J M and Hanuza J 2008 *Phys. Rev. B* **78** 064116
[18] Zhai S, Xue W, Yamazaki D, Shan S, Ito E, Tomioka N, Shimojuku A and Funakoshi K I 2011 *Phys. Chem. Miner.* **38** 357
[19] Qin F, Wu X, Zhai S M, Qin S, Yang K, Chen D L and Li Y C 2014 *Phase Transit.* **87** 1255
[20] Frost R L, Palmer S J, Xi Y, Čejka J, Sejkora J and Plášil J 2013 *Spectrochim. Acta. A* **103** 431
[21] Frost R L, Xi Y, Palmer S J and Pogson R E 2011 *Spectrochim. Acta. A* **83** 106
[22] Frost R L, Xi Y, Scholz R and Tazava E 2013 *J. Mol. Struct.* **1037** 148
[23] Frost R L, Scholz R, López A, Lana C and Xi Y 2014 *Spectrochim. Acta. A* **126** 164
[24] Frost R L and Palmer S J 2011 *Spectrochim. Acta. A* **78** 1250
[25] Frost R L, Xi Y, Scholz R, Belotti F M and Beganovic M 2013 *Spectrochim. Acta A* **110** 7
[26] Frost R L, Xi Y, Scholz R, Belotti F M and Filho M C 2013 *Spectr. Lett.* **46** 415
[27] Förtsch E B 1967 *Mineral. Mag.* **36** 530
[28] Bain D C 1970 *Mineral. Mag.* **37** 934
[29] Mills S J, Kampf A R, Raudsepp M and Christy A G 2009 *Mineral. Mag.* **73** 837
[30] Mao H, Xu J and Bell P 1986 *J. Geophys. Res.* **91** 4673
[31] Hammersley A P, Svensson S O, Hanfland M, Fitch A N and Hausermann D 1996 *High Pressure Res.* **14** 235
[32] Toby B H 2001 *J. Appl. Crystallogr.* **34** 210
[33] Birch F 1947 *Phys. Rev.* **71** 809
[34] Malavi P S, Karmakar S, Karmakar D, Mishra A K, Bhatt H, Patel N N and Sharma S M 2013 *J. Phys.: Condens. Mat.* **25** 045402
[35] Kugel G E, Bréhat F, Wyncke B, Fontana M D, Marnier G, Carabatos-Nedelec C and Mangin J 1988 *J. Phys. C: Solid State Phys.* **21** 5565
[36] Frost R L, Xi Y, Beganovic M, Belotti F M and Scholz R 2013 *Spectrochim. Acta A* **107** 241
[37] Breitinger D K, Brehm G, Mohr J, Colognesi D, Parker S F, Stolle A, Pimpl T H and Schwab R G 2006 *J. Raman Spectrosc.* **37** 208
[38] Frost R L, Xi Y, Scholz R, López A, Lima R M F and Ferreira C M 2013 *Vib. Spectrosc.* **67** 14
[39] Frost R L, Xi Y, Palmer S J and Pogson R E 2012 *Spectrochim. Acta A* **94** 1
[40] Gao J, Wu X, Qin S and Li Y C 2016 *High Pressure Res.* **36** 1
[41] Zhai S, Wu X and Ito E 2010 *J. Raman Spectrosc.* **41** 1011
[42] Hofmeister A M and Mao H K 2002 *Proc. Nati. Acad. Sci. U.S.A.* **99** 559
[43] Williams Q and Knittle E 1996 *J. Phys. Chem. Solids* **57** 417